Computers and Electronics in Agriculture 162 (2019) 951–961

Contents lists available at ScienceDirect

Computers and Electronics in Agriculture

journal homepage: www.elsevier.com/locate/compag

Original papers

Automated morphological traits extraction for sorghum plants via 3D point cloud data analysis

Lirong Xiang[a], Yin Bao[a], Lie Tang[a,*], Diego Ortiz[b], Maria G. Salas-Fernandez[b]

[a] Department of Agricultural and Biosystems Engineering, Iowa State University, Ames, IA 50011, United States
[b] Department of Agronomy, Iowa State University, Ames, IA 50011, United States

ARTICLE INFO

Keywords:
3D point cloud data
Phenotyping
Plant morphology
Skeletonization
Sorghum

ABSTRACT

The ability to correlate morphological traits of plants with their genotypes plays an important role in plant phenomics research. However, measuring phenotypes manually is time-consuming, labor intensive, and prone to human errors. The 3D surface model of a plant can potentially provide an efficient and accurate way to digitize plant architecture. This study focused on the extraction of morphological traits at multiple developmental timepoints from sorghum plants grown under controlled conditions. A non-destructive 3D scanning system using a commodity depth camera was implemented to capture sequential images of a plant at different heights. To overcome the challenges of overlapping tillers, an algorithm was developed to first search for the stem in the merged point cloud data, and then the associated leaves. A 3D skeletonization algorithm was created by slicing the point cloud along the vertical direction, and then linking the connected Euclidean clusters between adjacent layers. Based on the structural clues of the sorghum plant, heuristic rules were implemented to separate overlapping tillers. Finally, each individual leaf was automatically segmented, and multiple parameters were obtained from the skeleton and the reconstructed point cloud including: plant height, stem diameter, leaf angle, and leaf surface area. The results showed high correlations between the manual measurements and the estimated values generated by the system. Statistical analyses between biomass and extracted traits revealed that stem volume was a promising predictor of shoot fresh weight and shoot dry weight, and the total leaf area was strongly correlated to shoot biomass at early stages.

1. Introduction

Improving the efficiency of plant breeding and crop production is crucial to the success of meeting the increasing food and energy demands of over nine billion global population by 2050 (Tilman et al., 2011). High yielding, stress-tolerant plants could be developed more rapidly than is currently possible by analyzing the relationship between genotypes and phenotypes under various growth environments (Furbank and Tester, 2011). Boosted by technological developments such as high-throughput DNA sequencing, the efficiency of genotyping has been greatly improved (Phillips, 2010). However, the capability of phenotyping is still a bottleneck for dissecting the genetics of quantitative traits such as plant height, leaf angle, leaf area, and biomass (White et al., 2012). The conventional phenotyping practice tends to be time-consuming, labor-intensive, and prone to human errors. Thus, it is vitally important to develop techniques for collecting crop phenotypic data with higher accuracy and efficiency.

Though two-dimensional (2D) images have been widely used in image-based phenotyping techniques, 2D methods struggle to accurately reflect three-dimensional (3D) quantities (Gibbs et al., 2018; Kaminuma et al., 2004). Previous works has demonstrated that analyzing plants in 3D space offers greater robustness and accuracy (An et al., 2017; Apelt et al., 2015). In addition to the quantitative description, 3D imaging enables measurements of more traits than what is possible with 2D images such as the volume of fruits (Paulus et al., 2014a). To date, advanced computer vision techniques have employed 3D information to quantify plant traits (Li et al., 2014). Generally, there are two approaches for 3D image-based phenotyping. In one approach, 3D surface models are reconstructed by 2D images taken from multiple views, which is referred to as the passive methods. Stereo vision is one of the passive imaging techniques that reconstruct 3D canopies by synthesizing multi-view images. This method has been successfully used for canopy model reconstruction (Bao et al., 2019; Salas Fernandez et al., 2017) and growth estimation (Rovira-Más et al., 2005). However, the performance is affected by the lack of texture in the objects and sunlight variations (Frasson and Krajewski, 2010). Structure-from-

* Corresponding author.
E-mail address: lietang@iastate.edu (L. Tang).

https://doi.org/10.1016/j.compag.2019.05.043
Received 27 January 2019; Received in revised form 15 May 2019; Accepted 21 May 2019
Available online 24 May 2019

Motion (SfM) is another commonly used technique for 3D reconstruction due to the relatively high accuracy of the sensors (Bellasio et al., 2012; Nguyen et al., 2015), but its major limitation is the intensive computation required for reconstruction (Jay et al., 2015). Another approach to 3D-based plant phenotyping is an active method that directly acquires 3D distribution of plant canopies by using external light sources (Jiang et al., 2018). Several 3D sensors have been used for 3D modeling of plants and leaves, such as Light Detection and Ranging (LiDAR), Time-of-Flight (ToF) cameras, and 3D laser scanners. LiDAR applications include canopy reconstruction (Garrido et al., 2015), and the estimation of LAI (Tang et al., 2014), plant height (Sun et al., 2017), volume and biomass (Eitel et al., 2014; Rosell Polo et al., 2009)). ToF cameras have been used for crop recognition (Li and Tang, 2018), crop monitoring (Andújar et al., 2016a; Jiang et al., 2016), and plant traits measurement (Alenya et al., 2011; Chaivivatrakul et al., 2014). Finally, laser scanners have been successfully deployed for LAI mapping (Gebbers et al., 2011), plant organ classification (Paulus et al., 2013), and growth tracking of plants over time (Paulus et al., 2014b). High accuracy, high signal update rate, and strong robustness are the advantages of these devices, though, the major limitations are the high signal noise level and sensitiveness to environmental variations (e.g., sunlight, wind).

Recent advances in commercial-grade depth sensors provide a new solution for measuring plant architecture (Hu et al., 2018). The Microsoft Kinect v2 camera is one of the most commonly used depth sensors that, with upgraded color and depth resolutions, has performed well in plant phenotyping. McCormick et al. (2016) developed a 3D reconstruction system for sorghum (*Sorghum bicolor*) plants using a Kinect v2 camera with which plant architecture could be generated from a semi-automated data processing pipeline and shoot architecture phenotypes could be automatically measured. This work showed that measurements obtained with the Kinect depth camera are reliable for applications such as quantitative trait loci (QTLs) mapping. Andújar et al. (2016b) described a method for 3D modeling of cauliflower plants with a Kinect-based automated system. This method relied on the creation of a 3D point cloud in real time, and the subsequent generation of a solid surface model. In their work, significant correlations between measurements from the models and actual structural parameters were found.

Sorghum is the fifth most important grain crop, and a promising feedstock for biofuel production due to its excellent drought tolerance (Xin et al., 2008) and water use efficiency (Borrell et al., 2014). If phenotypes such as plant height, stem diameter, and leaf area can be deduced from the 3D plant architecture without destroying the sorghum plant, then detailed evaluations of these parameters through time can help study the genetic basis of complex traits over a variety of genotypes, and hence improve the efficiency of breeding programs (Li et al., 2014). Moreover, non-destructive biomass estimation can be important to dissect the genetic architecture and variability of sorghum biomass yield under different stress conditions. However, in reality, phenotyping sorghum plants via imaging remains a particularly challenging task due to the occlusions caused by overlapping leaves and tillers, often leading to the requirement of user interaction to facilitate the image analysis (Pound et al., 2014; Salas Fernandez et al., 2017). The overall goal of this study is to automatically extract sorghum plant architectural parameters via 3D point cloud analysis. The specific objectives are to: (1) reconstruct the 3D surface model of the imaged plants, (2) develop a robust data processing pipeline to characterize the plant architecture, (3) extract phenotypic data including plant height, stem diameter, leaf angle, and leaf area, and (4) explore the possibilities of using the extracted traits for plant biomass estimation.

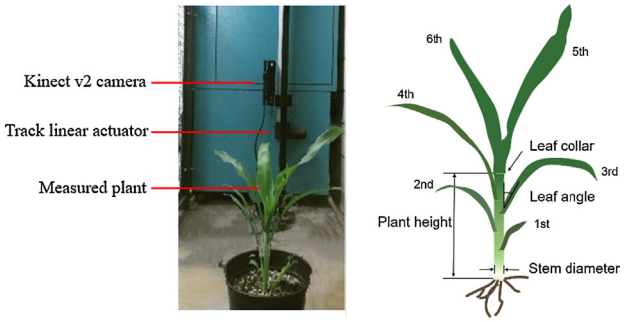

Fig. 1. (a). The setup of the image acquisition station. (b) Illustration of the manual measurements of plant height, leaf angle, and stem diameter.

2. Materials and methods

2.1. Experimental design and data acquisition

A non-destructive imaging system was developed for data acquisition. It consisted of a Kinect v2 camera, a vertical track linear actuator, and a computer station (Fig. 1). The Kinect v2 has a depth camera with a resolution of 512 × 424 pixels, an RGB camera of 1920 × 1080 pixels, and an infrared emitter. Kinect v2's depth measurement is based on Time-of-Flight (ToF) of light principle, where the distance between the emitter to the target is calculated from the travel time of the modulated light (Andújar et al., 2016a). The Kinect camera was mounted on a vertically oriented and tracked linear actuator. The sorghum plant was positioned 0.9 m away from the linear actuator, with the widest side of the canopy facing the camera. The system took RGB-D images at multiple heights while moving the camera at a speed of 40 mm/s. Starting from the same height, the system stored one image in every second with more than 90% of overlapped areas between consecutive images. A total of four images were saved for each plant based on the heights of the sorghum plants used in this project. Images were taken in the laboratory under typical office lighting conditions.

A total of 32 sorghum plants were grown in a growth chamber and studied to validate the system. These plants corresponded to four genotypes (PI 656029, 533839, 564163 and 655996) and eight biological replicates per genotype. The plants were sampled at multiple developmental timepoints: 21 (W3), 28 (W4), and 35 (W5) days after planting (DAP). Fig. 2 shows the point clouds of one of the sampled sorghum plants at different growth stages. Plants were transported manually from the growth chamber to the imaging station. After taking images, plants were manually measured with standard techniques to evaluate the performance of the system. The ground truth data were collected by the same person. Plant height was measured from the soil to the collar of the last fully expanded leaf using a measuring tape, stem diameter was measured using a caliper at the stem section right above the soil, and leaf angle was measured only for the leaves completely out of the whorl by a protractor (Fig. 1b). Each week, eight plants (two per genotype) were randomly selected and cut at the base of the stem for leaf area and biomass measurements. Leaf area was measured by an LI-3000C Area Meter, and fresh biomass was obtained using an electronic balance. Subsequently, the plant was dried in an oven with a temperature of 65°C until the sample reached a constant weight. Total dry weight was then recorded.

2.2. Image processing pipeline

An automatic image processing pipeline was developed for determining plant architecture and characterizing phenotypic parameters. It comprised three sections: point cloud preprocessing, stem and leaf segmentation, and morphological traits extraction (Fig. 3). Routines

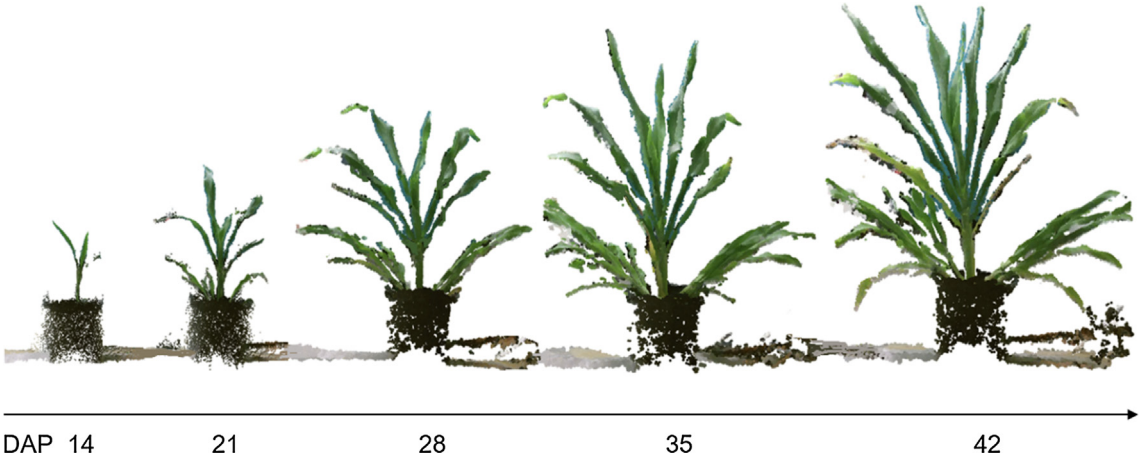

Fig. 2. Point clouds of a sorghum plant at different growth stages, where DAP stands for Days After Planting.

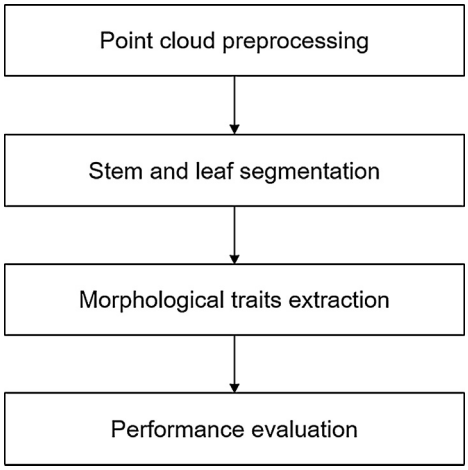

Fig. 3. Main steps of the proposed automatic processing pipeline.

from Point Cloud Library (Rusu and Cousins, 2011) and OpenCV library (Bradski and Kaehler, 2008) were adopted to implement those steps.

2.2.1. Point cloud preprocessing

An overview of the point cloud preprocessing is shown in Fig. 4. The four depth images taken at different heights were transformed into 3D point cloud using the equations listed as follows:

$$Z = d; \tag{1}$$

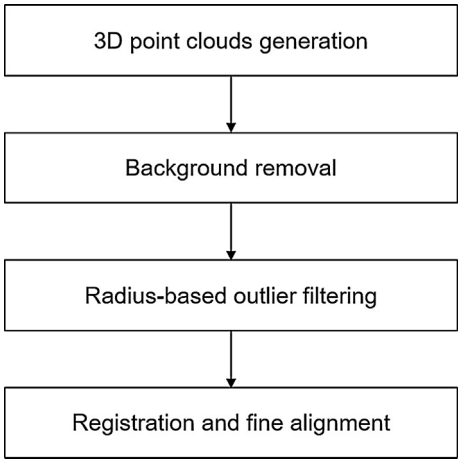

Fig. 4. Flowchart of the algorithm for point cloud preprocessing.

$$X = (x - c_x)/f_x * Z; \tag{2}$$

$$Y = (y - c_y)/f_y * Z; \tag{3}$$

where (x, y) is the 2D image point coordinates, d is the depth value of the 2D point. c_x and c_y represent the principal points along the camera X and Y axis. f_x and f_y are the focal lengths along the camera X, Y axis, respectively. (X, Y, Z) is the 3D coordinates of the corresponding point.

The point cloud data generated by the system contain some background objects (e.g., the supporting structure, the door, and walls of the room) which was removed by filtering out the 3D points outside a predefined bounding box containing the plant. The algorithm checks the X, Y, and Z coordinates of each point in the point cloud. Fig. 5a shows the results after background removal, where the point clouds obtained from different heights are visualized with different colors.

Due to the limitation of the sensor, the raw data of the sorghum point cloud always contains a few sparsely distributed noise points which commonly have low point density. A radius-based outlier removal filter was implemented to clean the noise points. This filter takes into account the number of neighboring points (K) within a user-defined search radius r of all points, a point will be removed as noise if less than K neighbors are found (Dziubich et al., 2016). We selected r = 5 mm and K = 5 which effectively reduced the number of noise points without losing true surface points.

After the background and noise removal, multiple neighboring point clouds were incrementally registered into a single point cloud (Fig. 5b) by using the Iterative Closest Point (ICP) algorithm. The ICP algorithm aligns two point clouds by iteratively minimizing the Euclidean distances between corresponding points (Holz et al., 2015). The multi-view point cloud registration was done by finding the best transformation matrix between each consecutive clouds and converging these transformation matrices towards the first cloud's frame.

2.2.2. Stem and leaf segmentation

The phenotypic data extraction of the plant organs (i.e., leaves and stems) was based on segmentation. Previous work has developed and validated methods for plant components segmentation. One of them was to first remove the stem, and then separate every single leaf by clustering methods (Lu et al., 2017). However, this was based on a relatively simple plant architecture with leaves that were spatially separated from each other after filtering the stem. Another method used machine learning approaches to classify each point by point-level 3D features (McCormick et al., 2016; Sodhi et al., 2017), but the approach needed a manually labeled subset for training the classifier, which was time-consuming. The plants used in our experiment not only had leaves but also tillers close to the stem, and the leaves at the top of the canopy remained connected. To overcome these challenges, a skeletonization

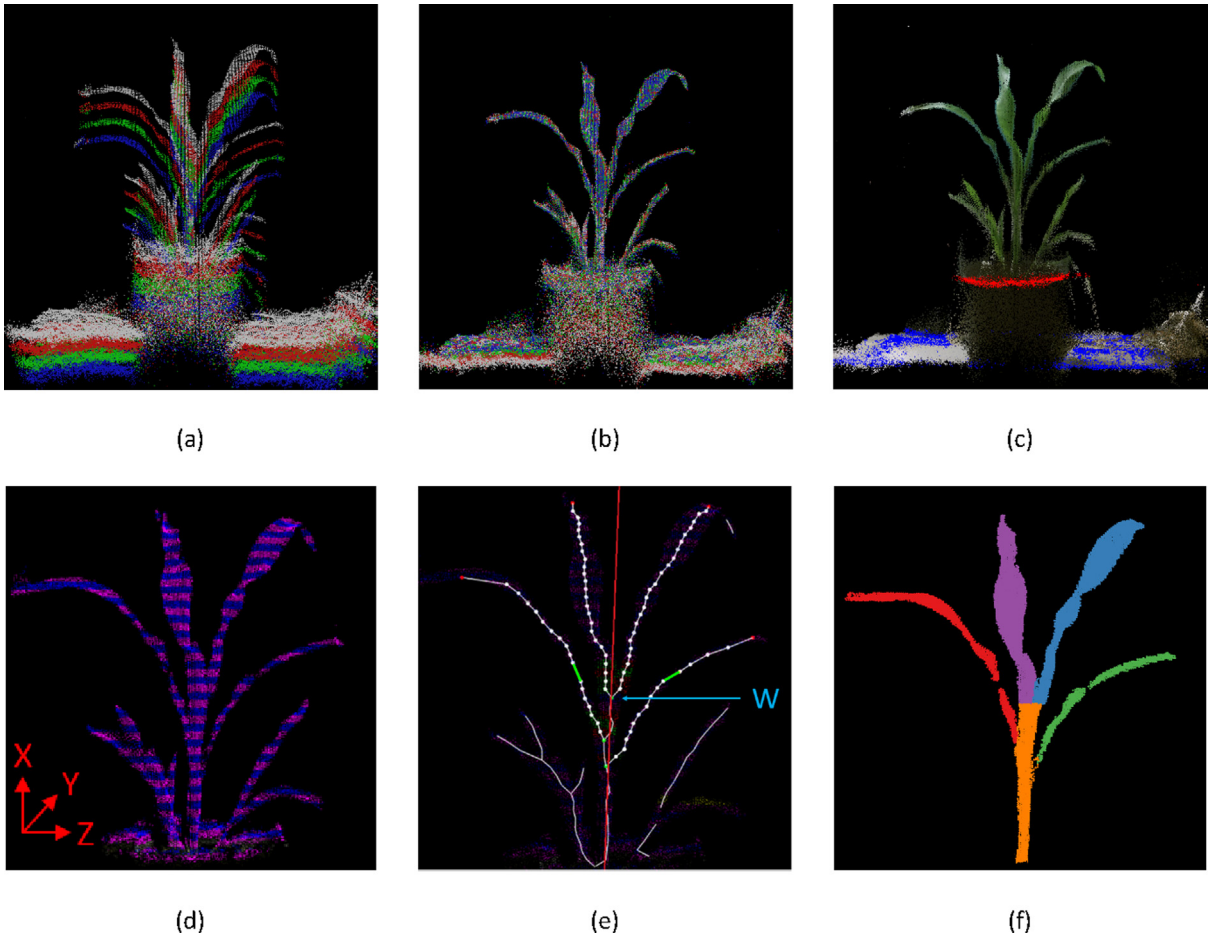

Fig. 5. Image processing pipeline: (a) Point clouds sampled from multiple heights. (b) Registered point cloud. (c) Ground and soil detection. Blue points are ground inliers and red points are soil inliers. (d) Sliced point cloud. (e) Hierarchical slice representation. The green point, red point, and white point represent junction, leaf tip, and internal node, respectively. The green lines are the reconnected skeleton of the broken leaves, and the red line denotes the stem central line. W stands for the positions of the junction node with the largest x value. (f) Stem and leaf segmentation. Different plant organs are visualized with different colors. (For interpretation of the references to colour in this figure legend, the reader is referred to the web version of this article.)

method was implemented to help build the structural clues of the whole plant. The algorithm was developed to first search for the stem by Hough line transform, and then segment each individual leaf.

Step 1: soil detection

The soil detection started with ground detection and the subsequent soil level estimation based on the ground level and the pot height. For ground detection, the Random Sample Consensus (RANSAC) algorithm (Fischler and Bolles, 1981) was used to fit a plane model. The method was applied to the full point cloud to find all the points that supported a plane model. Similarly, after ground detection, a soil detection process based on the RANSAC method was employed. We defined the direction perpendicular to the ground plane pointing upwards as the X-axis. The pot height was 0.20 m and the soil was always inside the pot. The soil detection only considered those points with an X-value from X_{ground} + 0.15 m to X_{ground} + 0.20 m, thus increasing the ratio of soil to all the points and improving the detection accuracy. The inliers of the plane model were extracted as the soil and the soil level X_{soil} was estimated by averaging the X coordinates of all the inliers. The points above the soil were extracted as the region of interest and were used for the phenotypic traits extraction. Fig. 5c shows the point cloud with the ground inliers in blue and soil inliers in red.

Step 2: point cloud skeletonization

We introduced a point cloud skeletonization method to analyze the sorghum plant architecture. The 3D skeletonization algorithm was developed by slicing the point cloud along the X-axis (Fig. 2d) and linking the connected Euclidean clusters (Rusu and Cousins, 2011) between adjacent layers. The generated skeleton was mapped to an undirected graph with each node denoting the cluster's centroid and the edge weight denoting the Euclidean distance between the two connected nodes. For each node, we stored its neighbors and indices of the points in the cluster. Due to inter-plant occlusion and boundary noises, the initial skeleton graph may include loops and redundant spurious branches, thus clean skeletons were extracted by removing loops using Kruskal's algorithm (Kruskal, 1956) and pruning spurious branches. The process of skeleton pruning was based on thresholding, if a branch contained less than α nodes, it was discarded as a spur. The value of α was selected as 3, since all short branches were removed using this threshold value for our dataset. Fig. 5d shows the sliced point cloud and Fig. 5e shows its graphical representation after the skeleton graph pruning.

In the graph, every node has references to its neighbors, where the node is regarded as a parent if it has a smaller x value than its neighbor or otherwise, it is considered as a child. With this hierarchy, all the nodes can be categorized into three cases:

(1) Leaf tip (T): node with one neighbor.
(2) Internal node (I): node with two neighbors – usually has one child and one parent node.

(3) Junction (J): node with more than two neighbors – normally has only one parent and at least two child nodes.

It was observed that the junctions near the stem were always higher than the leaf collars because the slice near the leaf collar always contained both the stem and leaf base. To solve this problem, a skeleton refinement algorithm was implemented. Each branching node was split into two nodes by applying 2-means clustering to the point cluster associated with the original node. The splitting process continued until the distance between the two new nodes was less than a user-defined threshold. Based on trial and observation, we set the threshold to 0.02 m, which was approximately the stem diameter.

Step 3: stem identification

The stem in the merged point cloud could be approximately modeled as an elliptical cylinder (Chaivivatrakul et al., 2014; Frasson and Krajewski, 2010). However, if we directly searched for the points in the merged cloud that could be considered as a cylinder, the results always contained the part of rolling and straight young leaves (plant whorl). The whorl position was identified by searching for the junction node with largest x value in the skeleton (Fig. 2e labels the node as *W*). To distinguish whorl from the shoot cylinder, the stem segmentation only considered those points lower than the plant whorl. After that, the 3D Hough transform (Dalitz et al., 2017) was applied to detect the central line of the cylinder model and the direction vector v of the line was calculated. The 3D Hough transform is an iterative voting process which selects the line with the most votes and removes the corresponding points after each iteration. Once the stem center line has been identified, the points corresponding to the shoot cylinder can be extracted by a thresholding-based strategy, i.e., the stem inliers are the points within a suitable radius from the central line (Fig. 5e shows the stem center line in red and Fig. 5f shows the stem inliers in orange).

Step 4: leaf segmentation

Leaf segmentation could be considered as a graph partitioning problem. We reconstructed each partial segment by iteratively traversing the graph from a leaf tip along a connected path of internal nodes until encountering a junction, the results of which can contain both leaves and tillers. Since sorghum leaves are very thin, the corresponding point cloud could be sparse if the camera captures the side view of a leaf, thus the filtering process described in Section 2.2.1 may cause disconnections of a single leaf. Before partial segmentation, a reconnection of the skeleton was employed to connect the broken leaves. The approach checked each one-degree node. If its distance to the nearest one-degree neighbor is less than the threshold (0.03 m in our case, which is determined heuristically), then the two nodes were connected. Fig. 5e shows the reconnected edge in green. Considering that leaves emerged from the shoot cylinder while tillers originated from the soil, we selected the partial segments connected with the stem as leaf candidates. Fig. 5e shows that each individual leaf starts with a green node and ends with a red node. The stem and leaf segmentation is summarized in Algorithm 1.

Algorithm 1: Skeletonization algorithm for Stem and Leaf Segmentation

Input: C: The registered and filtered point cloud.
Output: Skeleton graph of the point cloud and determination of individual plant organs.

1: $P_{original}$ = segment(C);
The region of interest, i.e., the sorghum plant, is extracted from the registered cloud by filtering out the points lower than the soil level.

2: $G_{initial}$ (V, E) = initialize - skeleton($P_{original}$);
Compute the initial skeleton of the segment P and transform the 3D skeleton into a graph representation

3: $G_{refined}$(V, E) = refine - skeleton ($G_{initial}$)
Remove loops using Kruskal's algorithm and prune short branches using a threshold of α nodes

4: {T, I, J} ← VCategorize the set of nodes V into leaf tips (T), internal nodes (I) and junctions (J)
based on the number of neighbors of each node

5: W, $P_{part\text{-}plant}$ ← detect - whorl ($G_{refined}$)
Find the highest junction in J, label the junction node W as 'plant whorl', extract the points lower than the whorl as a cluster P_1, which will be used for stem segmentation

6: P_{stem} = stem - segmentation ($P_{part\text{-}plant}$)
Detect the central line of the shoot cylinder in $P_{part\text{-}plant}$, identify the stem inliers (P_{stem}) from the data by extracting the points within a suitable radius from the central line.

7: $G_{reconnected}$ = skeleton - reconnection ($G_{refined}$)
If the distance between a one-degree node and its nearest one-degree neighbor is $\leq \beta$, connect the two nodes.

8: {X_1, X_2, …, X_n} = partial - segment ($G_{reconnected}$)
Partition the skeleton graph into 1D partial segments such that each segment starts with T and ends with J. Each partial segment is defined as X = {N_1, N_2, … , N_m}, where m is the number of nodes in the segment X.

9: {L_1, L_2, …, L_n} ∈ {X_1, X_2, …, X_n}
If one endpoint of a partial segment $X_i \in P_{stem}$, label the segment as a leaf (L_j).

2.2.3. Morphological traits extraction

Five phenotypic parameters were extracted from the point clouds: plant height, stem diameter, stem volume, leaf angle, and leaf area. The multiple morphological traits obtained from the point clouds can be classified into two categories: (a) holistic traits and (b) organ-level traits. Holistic traits quantify the overall plant architecture, such as plant height and total leaf area. Organ-level traits analyze the individual organs of the plants, including stem diameter, leaf angle, and area of individual leaves. Fig. 6 shows the definitions and principles of the measured phenotypes mentioned above.

Plant height: Plant height is defined as the distance from soil to the collar of the youngest fully expanded leaf, which is a useful and frequently measured trait in agronomic research (Neilson et al., 2015). In the graphical representation, the beginning of the stem was defined as the point where the stem emerges from the soil, and the end was defined as the second junction node from the top (where the corresponding leaf was typically fully expanded). The algorithm finds the second highest junction node (leaf collar) by checking the X coordinate of each node with those of two neighbors in the skeleton graph. Therefore, the plant height can be estimated as the distance from the node to the soil level along the stem direction using:

$$H = \frac{X - X_{soil}}{cos\varnothing} \quad (4)$$

where ∅ is the angle between the stem center line and the Y-Z plane. X and X_{soil} denote the x-coordinate of the leaf collar and x-coordinate of the soil, respectively.

Stem diameter: Stem diameter was measured close to the soil to provide consistent and representative measurements of the entire stem. In the point cloud of the sorghum plant, the stem inliers immediately above the soil may not be complete due to occlusion by tillers, so eight slices of stem inliers whose distances to the soil ranged from 2 cm to 10 cm were used for stem diameter extraction (the thickness of each slice was 1 cm). The stem diameter was determined based on sorghum stem's roughly elliptical cross-section, hence the points of each slice were projected orthogonally onto the Y-Z plane (Fig. 6a). Subsequently, ellipse fitting operation was applied to the projected points using an OpenCV library's build-in function (Bradski and Kaehler, 2008), which works by first finding the contour and then approximating an ellipse by minimizing the algebraic distance to its constraints (Fitzgibbon et al., 1999). The major axis of the fitted ellipse represents the stem width along the major axis of the elliptical cross-section (Fig. 6b), therefore, the stem diameter can be calculated by averaging the major axes of all the ellipses of the stem slices.

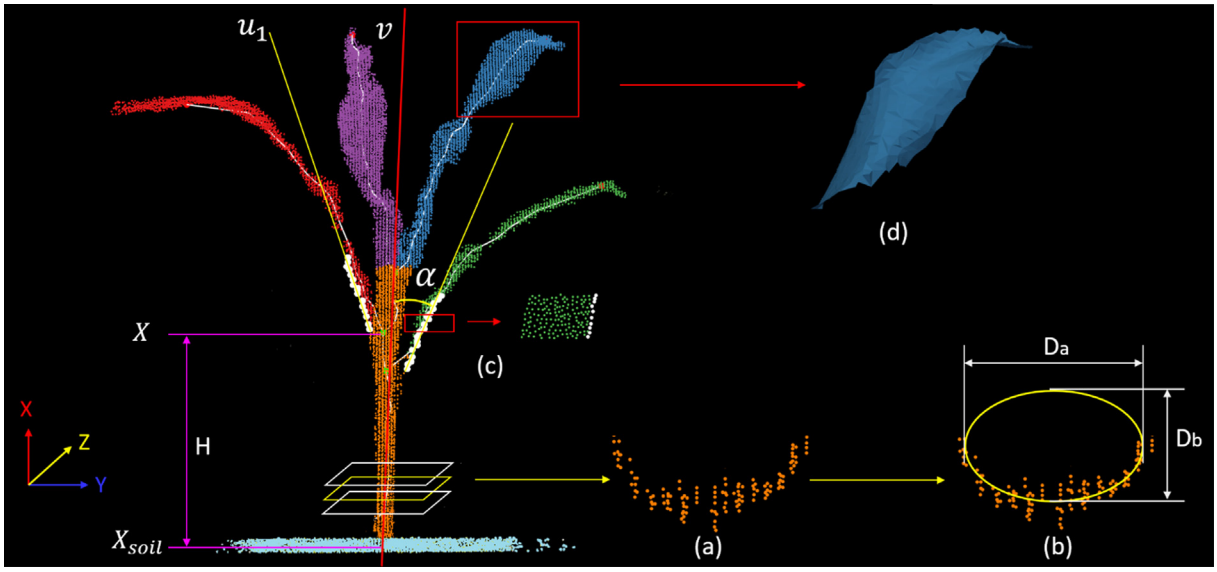

Fig. 6. Phenotypic parameters: H – plant height; D_a – stem diameter (major axis of the fitted ellipse); D_b – minor axis of the fitted ellipse; α – leaf angle; (a) Orthogonal projection on Y-Z plane of the sliced stem point cloud; (b) Projected point cloud with ellipse fitting; (c) the outer edge of the leaf point cloud; (d) triangular mesh of leaf surfaces. In the figure, u1 and v are the direction vectors of the selected edge points and the stem cylinder, respectively. X and Xsoil denote the X coordinates of the leaf collar and the soil, respectively.

Stem volume: Once the stem diameter has been extracted, the stem volume could be estimated based on the formula for the volume of an elliptical cylinder using:

$$V = \frac{\pi \times D_a \times D_b \times H}{4} \quad (5)$$

where H is the plant height, D_a and D_b denote the average major axis and minor axis of the fitted ellipses, respectively.

Leaf angle: Leaf angle is defined as the inclination between the leaf blade midrib and the stem. For leaf angle extraction, we used the leaf points within a radius of 0.06 m (which was chosen empirically) from the central line of the stem cylinder model. To estimate the orientation of the leaf, the outer edge of the point cloud of the selected portion was first recognized (Fig. 6c). Since the direction in which the leaves emerge was perpendicular to the sensor viewing direction in our experimental setup, the outer edge of the leaf seen by the depth sensor approximately represented the leaf blade midrib. Let I(x, y, z) denote the edge points of the leaf. To recognize the orientation of the leaf, Principle Component Analysis (PCA) was performed on I. The PCA transformation computes a covariance matrix of I, which can be decomposed to a set of eigenvectors (u_1, u_2, u_3) and eigenvalues (λ_1, λ_2, λ_3). The eigenvector u_1 with the highest eigenvalue identifies a direction accounts for the greatest possible variance in the data set, hence providing an estimation of the overall orientation of the leaf. The Hough line fitting in stem segmentation process provided a direction vector (v) of the center line of the cylinder model of the stem. Then, the leaf angle was calculated as the angle between u_1 and v. An example of leaf angle measurement is shown in Fig. 6, where white points are the edge points, and the yellow lines represent the direction of the major eigenvectors.

Leaf area and total area: To reconstruct the leaf surfaces, a greedy surface triangulation algorithm (Marton et al., 2009) was implemented to generate a triangle mesh based on a set of inliers of each individual leaf. The triangulation was performed based on projections of the local neighbors of a point along its normal. Fig. 6d shows the reconstructed triangle mesh of a plant leaf. Leaf area was obtained by summing the triangle area of each leaf's surface mesh, and the total area included the surface area of all individual leaves and tillers.

2.3. Performance evaluation

Linear regression analyses were performed between the manual measurements and the system-derived measurements for all extracted parameters. The following statistics were calculated for performance evaluation: correlation coefficient (r), root mean square error (RMSE, Eq. (1)), and mean absolute error (MAE, Eq. (2)).

$$RMSE = \sqrt{mean(est - act)^2} \quad (6)$$

$$MAE = mean(|est - act|) \quad (7)$$

where *est* and *act* denote estimated values from the system and actual values from manual measurements, respectively.

The total area and stem volume obtained from the system were analyzed and compared with the wet and dry biomass using linear regression. The r value was calculated to evaluate the relationships between the actual parameters and those extracted from the system.

3. Results and discussion

Fig. 7 shows the 3D point cloud and the segmentation results of plant architectures for sorghum plants at different growth stages, where the individual leaf skeletons are visualized with random colors. The visualization of the 3D surface model appeared realistic, the result of the individual leaf segmentation matched the ground truth. It was noticed that the bottom leaf of the first plant in Fig. 7c was missed, this was mainly because the too much overlap between the leaf and the tillers, as a result of which the skeletons of the leaf were removed as a part of the tillers. Overall, the results demonstrate that the segmentation algorithm was effective to extract each individual leaf from the 3D point cloud of the sorghum plants.

3.1. Accuracy assessment

Comparisons of manual measurements and system-derived measurements of phenotypic parameters are shown in Fig. 8. The results show that 3D point cloud analysis is well suited for measuring the parameters inspected in this study, especially for stem diameter, leaf angle, and individual leaf area. The system-derived plant height is well correlated with the manual measurements (r = 0.81). A strong

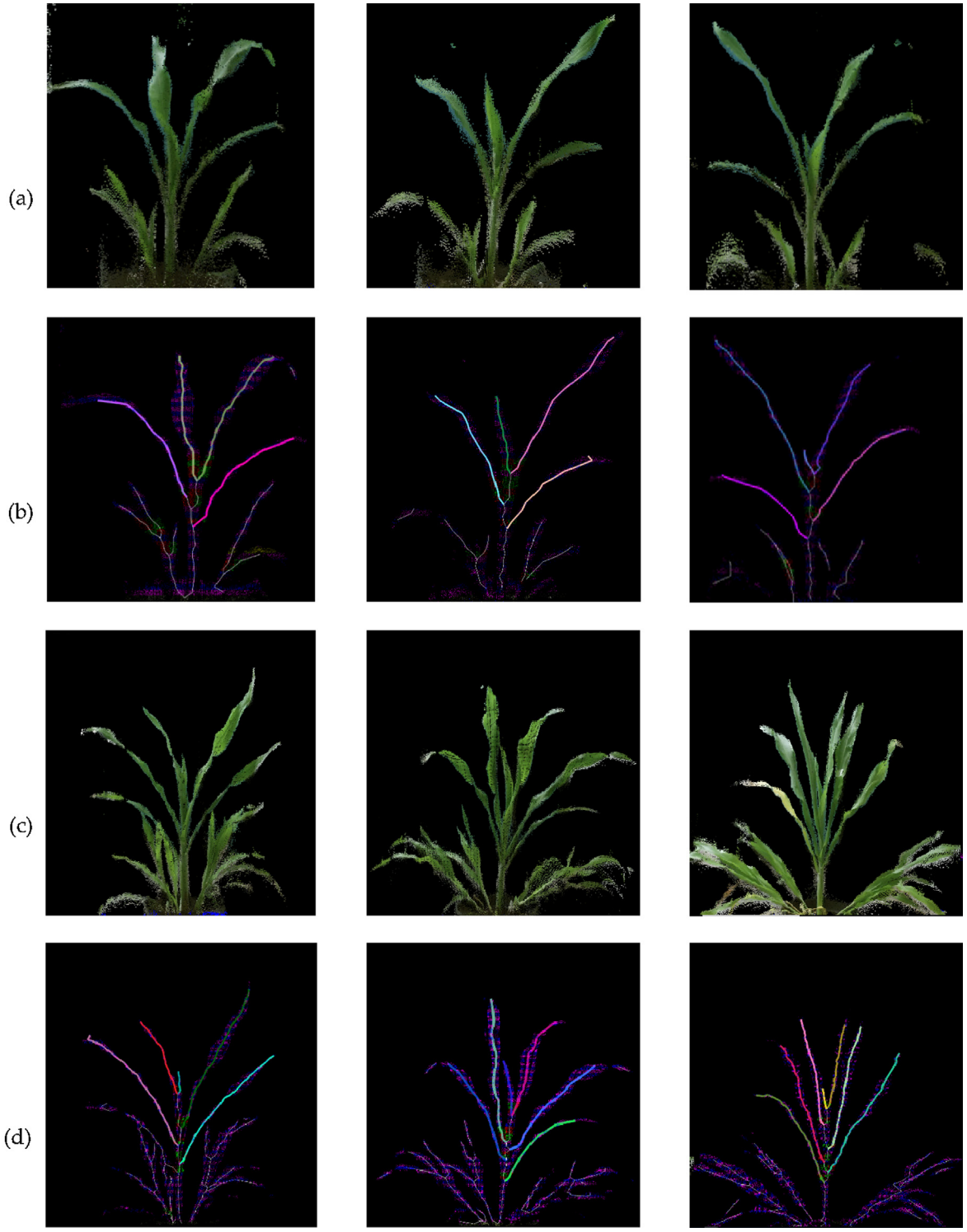

Fig. 7. (a) Point clouds of plants at W3. (c) Point clouds of plants at W4 and W5. (b)–(d) Skeletons of plants with each leaf skeleton visualized with different colors. (For interpretation of the references to colour in this figure legend, the reader is referred to the web version of this article.)

correlation (r = 0.93) was obtained for the stem diameter with an RMSE of 1.61 mm and an MAE of 1.10 mm. The leaf angle yielded a coefficient of correlation of r = 0.84. The RMSE and MAE for the leaf angle were 2.64° and 2.24°, respectively. The image-derived leaf area was highly correlated with the manual measurement (r = 0.94), and the RMSE and the MAE were 12.94 cm^2 and 15.00 cm^2, respectively.

The plant height was manually measured using a tape from the soil to the collar of the last fully expanded leaf. However, the Kinect camera did not have the sufficient depth resolution to distinguish the leaf collars from other parts, thus making it challenging to detect collars in the point cloud. We defined the second highest junction as the leaf collar in our method, whereas for some sorghum plants, the youngest fully expanded leaves were located at the third highest junction, hence resulting in a relatively higher error for the plant height. A more precise way to find the collar of the last fully expanded leaf in the point cloud is needed to improve the accuracy of the plant height estimation. Furthermore, a more objective and clearer mathematical definition of the plant height needs to be investigated.

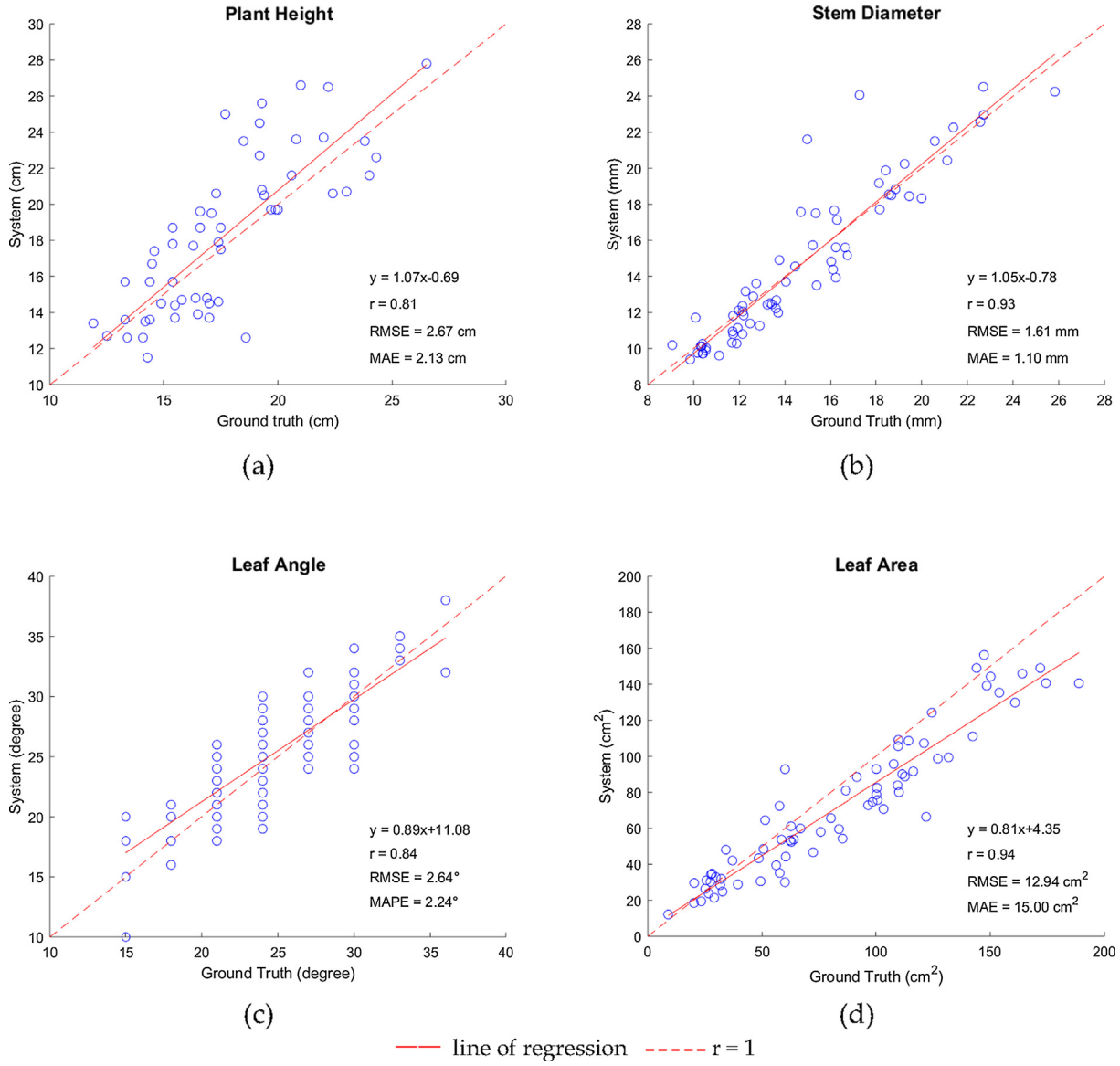

Fig. 8. Linear regression results between the image-derived measurements and the manual measurements for plant height (a), stem diameter (b), leaf angle (c), and leaf area (d).

For stem diameter, the regression line of the data points matched well with the diagonal reference line (r = 1) (Fig. 8b), validating the point cloud processing method as an accurate technique for measuring sorghum stem diameter. The correlation coefficient (0.93) indicated a strong correlation between the estimated stem diameter of sorghum plants and the reference value. Given the average sorghum stem diameter was 14.78 mm, the MAE (1.10 mm) presented an error rate of 7.4% of the average. It should be noticed that there were two outliers, which occurred because the tillers were located very close to the stem. Since the bottom slices were used for the stem cross-section calculations, the tiller proximity caused an overestimation of the stem diameter.

In spite of the narrow range of leaf angle observed in this experiment (15° ~ 36°), both the RMSE and MAE were less than 3.00°, indicating that edge-based angle extraction via point cloud is well suited for determining the leaf angle. The random errors could be caused by two factors. First, the leaf angle extraction algorithm assumed that leaves were well aligned in the imaging plane, while in reality there existed some leaves distributed in other directions, resulting in that the outer edge points in the point cloud did not precisely denote the direction of the midrib. Second, some crooked and curled leaves did not have a smooth outer edge, which resulted in a large variance in edge point, leading to an inaccurate estimation of the leaf orientation with the use of the major eigenvector.

Overall, the leaf area derived from the system underestimated the actual leaf area, as most data points showed in Fig. 8d were below the diagonal line. This is mainly caused by rolling and hidden parts of the upper leaves, since the Kinect sensor acquired point clouds only from the visible parts, resulting in a lack of information of leaves within the whorl. The leaf area was further underestimated during the process of triangulation, which tends to smooth the small variations in leaf surface and eliminate the local wrinkled structures particularly near the leaf tip and boundaries. This can be reduced by a more accurate triangulation methodology to reconstruct more details of leaf surfaces. Additionally, leaf occlusion and leaf rolling near the tips can also introduce errors. Nevertheless, the r value of 0.94 revealed that leaf area estimates were significantly correlated with the ground truth and the Kinect sensor can be an effective tool to measure leaf area.

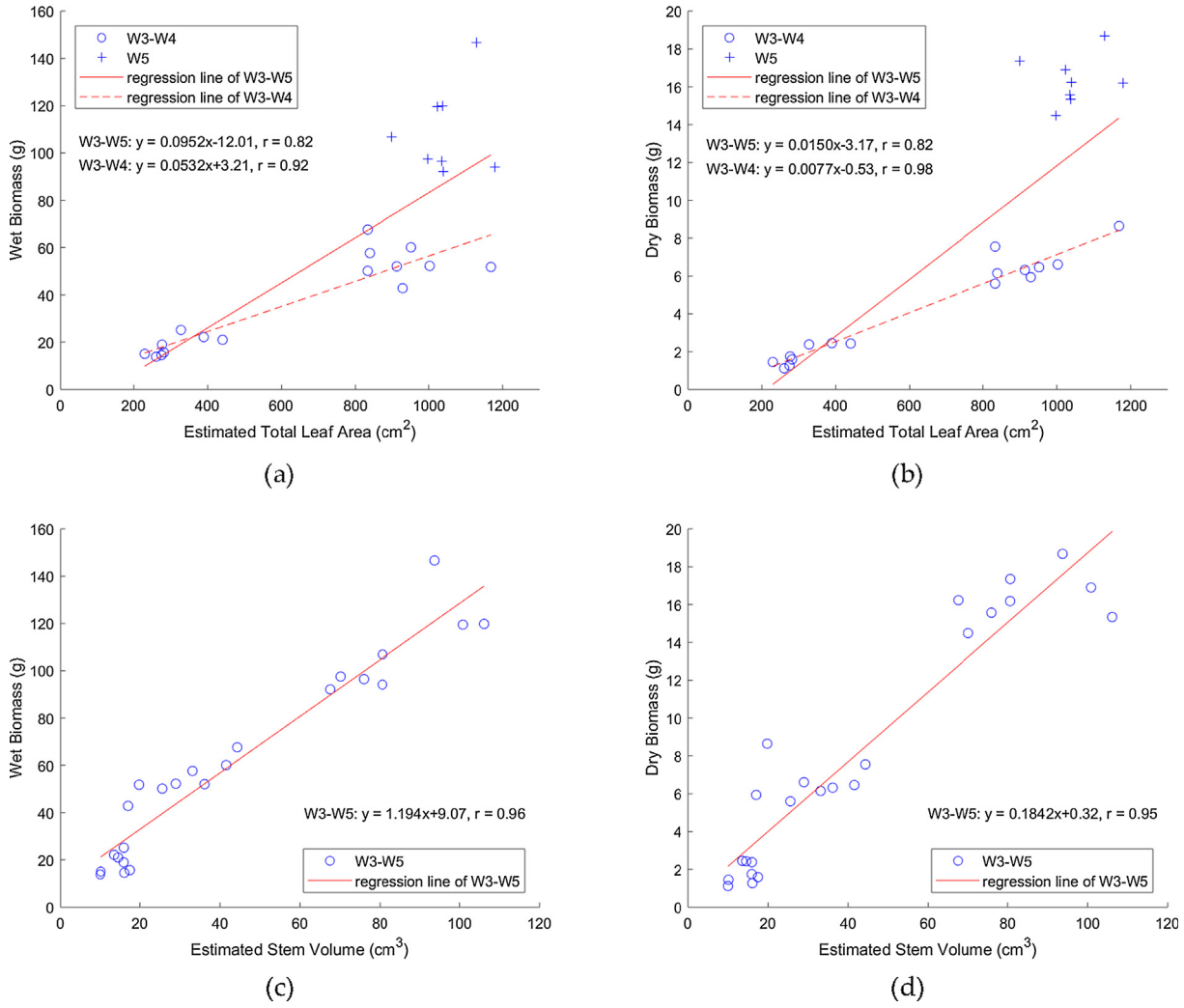

Fig. 9. Correlation of system-derived traits and biomass: (a) Estimated total leaf area and wet biomass. (b) Estimated total leaf area and dry biomass. (c) Estimated stem volume and wet biomass. (d) Estimated stem volume and dry biomass.

3.2. Performance of biomass estimation

In addition to capturing morphological traits of plant architecture, the biomass prediction (fresh weight and dry weight) based on the extracted traits was investigated. Fig. 9 showed the linear regression between the biomass and the system-derived traits. The total leaf area achieved similar results with wet and dry biomass from stage W3 to W5 (both r = 0.82). The stem volume had strong correlations with the wet biomass (r = 0.96) and dry biomass (r = 0.95). The values showed the promising potential of the Kinect v2 in biomass prediction.

Though some previous studies reported the total leaf area had significant correlations with fresh weight and dry weight (Neilson et al., 2015; Yang et al., 2014; Zhang et al., 2017), the r values were not high when we using the data from stage W3 to W5. The variation in growth status among individual plants during W5 were larger than that during the other two growth periods (Fig. 9a and b). To address this problem, a linear regression was performed on the data in W3 and W4. When only the early stages were considered, the linear relationship between the total leaf area and the sorghum biomass showed noticeable improvement, with an r of 0.92 for the wet biomass and 0.98 for the dry biomass.

Compared with the total leaf area, the stem volume showed a significant improvement in correlation with the actual sorghum biomass, which added both stem height and stem size information to the model. Consistent with this, several studies have shown that biomass is related to stem height and diameter. Some researchers (George-Jaeggli et al., 2011) found that plant height can affect the biomass production of sorghum, and the reduced plant height was mainly due to a reduction in stem length to the collar of the flag leaf. Other studies have also shown that sorghum biomass has a positive relationship with stem diameter in both well-watered (Clough and Hunter, 2003) and drought-stressed conditions (Almodares et al., 2013).

For biomass (both fresh and dry weight) prediction, a noticeable improvement was achieved by adding stem-related features to the model. The stem volume generally achieved a stronger correlation with biomass than did the total leaf area. The total leaf area was more significant in predicting sorghum biomass at early stages (W3-W4) because of the more significant contribution of stem growth to biomass weight at later stages (W5). Therefore, it is possible to use Kinect v2 to estimate sorghum plant biomass, which can replace the intense labor needed to collect morphological traits related to biomass. Depth imaging is non-invasive to plants, and thus, it can be performed at different growth stages without damaging the plants.

4. Conclusions

We developed a low-cost machine vision system based on a commodity depth camera. The system was capable of vertically acquiring sequential side-view images of sorghum plants grown under controlled conditions at multiple developmental timepoints. A skeletonization

algorithm was implemented to detect the individual leaves and distinguish the tillers by analyzing the 3D point cloud using a graph-based approach. The system was used to identify the sorghum plant architecture and characterize multiple important parameters. Automated measurements from the 3D surface model showed agreement with the corresponding manual measurements, validating the accuracy and utility of the system. In addition, both the total leaf area and stem volume showed potential for wet and dry biomass prediction ($r = 0.82 \sim 0.98$). As such, depth imaging provides an efficient and economical solution for plant architecture characterization and phenotypic traits extraction, and hence can facilitate genomic studies and plant breeding programs. Future work will focus on improving the algorithms to address leaf occlusions better, and to adapt this approach to different growth environments and field scenarios.

Acknowledgements

This project was sponsored by the Plant Sciences Institute at Iowa State University. This material is based upon work supported by the National Science Foundation (Grant No. 1149603 to MGSF). MGSF was supported by the United States Department of Agriculture, National Institute of Food and Agriculture (Project #IOW04314). We thank Juan Panelo, Facundo Curin and Ezequiel Delfino for their contributions to the imaged and manual phenotypic data collection.

Declaration of Competing Interest

The authors declare no conflict of interest.

References

Alenya, G., Dellen, B., Torras, C., 2011. 3D modelling of leaves from color and ToF data for robotized plant measuring. In: 2011 IEEE International Conference on Robotics and Automation. IEEE, pp. 3408–3414. https://doi.org/10.1109/ICRA.2011.5980092.

Almodares, A.A., Hotjatabady, R.H., Mirniam, E., 2013. Effects of drought stress on biomass and carbohydrate contents of two sweet sorghum cultivars. J. Environ. Biol. 34, 585–589.

An, N., Welch, S.M., Markelz, R.J.C., Baker, R.L., Palmer, C.M., Ta, J., Maloof, J.N., Weinig, C., 2017. Quantifying time-series of leaf morphology using 2D and 3D photogrammetry methods for high-throughput plant phenotyping. Comput. Electron. Agric. 135, 222–232. https://doi.org/10.1016/j.compag.2017.02.001.

Andújar, D., Dorado, J., Fernández-Quintanilla, C., Ribeiro, A., Andújar, D., Dorado, J., Fernández-Quintanilla, C., Ribeiro, A., 2016a. An approach to the use of depth cameras for weed volume estimation. Sensors 16, 972. https://doi.org/10.3390/s16070972.

Andújar, D., Ribeiro, A., Fernández-Quintanilla, C., Dorado, J., 2016b. Using depth cameras to extract structural parameters to assess the growth state and yield of cauliflower crops. Comput. Electron. Agric. 122, 67–73. https://doi.org/10.1016/J.COMPAG.2016.01.018.

Apelt, F., Breuer, D., Nikoloski, Z., Stitt, M., Kragler, F., 2015. Phytotyping 4D : a light-field imaging system for non-invasive and accurate monitoring of spatio-temporal plant growth 693–706. https://doi.org/10.1111/tpj.12833.

Bao, Y., Tang, L., Breitzman, M.W., Salas Fernandez, M.G., Schnable, P.S., 2019. Field-based robotic phenotyping of sorghum plant architecture using stereo vision. J. F. Robot. 36, 397–415. https://doi.org/10.1002/rob.21830.

Bellasio, C., Olejníčková, J., Tesař, R., Šebela, D., Nedbal, L., Bellasio, C., Olejníčková, J., Tesař, R., Šebela, D., Nedbal, L., 2012. Computer reconstruction of plant growth and chlorophyll fluorescence emission in three spatial dimensions. Sensors 12, 1052–1071. https://doi.org/10.3390/s120101052.

Borrell, A.K., Mullet, J.E., George-Jaeggli, B., van Oosterom, E.J., Hammer, G.L., Klein, P.E., Jordan, D.R., 2014. Drought adaptation of stay-green sorghum is associated with canopy development, leaf anatomy, root growth, and water uptake. J. Exp. Bot. 65, 6251–6263. https://doi.org/10.1093/jxb/eru232.

Bradski, G.R., Kaehler, A., 2008. Learning OpenCV : computer vision with the OpenCV library, 1st ed. O'Reilly.

Chaivivatrakul, S., Tang, L., Dailey, M.N., Nakarmi, A.D., 2014. Automatic morphological trait characterization for corn plants via 3D holographic reconstruction. Comput. Electron. Agric. 109, 109–123. https://doi.org/10.1016/J.COMPAG.2014.09.005.

Clough, A., Hunter, M.N., 2003. Stem diameter: a rapid and accurate parameter for monitoring growth of sorghum. Proc. Aust. Agron. Conf. Aust. Soc. Agron.

Dalitz, C., Schramke, T., Jeltsch, M., 2017. Iterative hough transform for line detection in 3D point clouds. Image Process. Line 7, 184–196. https://doi.org/10.5201/ipol.2017.208.

Dziubich, T., Szymański, J., Brzeski, A., Cychnerski, J., Korłub, W., 2016. Depth images filtering in distributed streaming. Polish Marit. Res. 23, 91–98. https://doi.org/10.1515/pomr-2016-0025.

Eitel, J.U.H., Magney, T.S., Vierling, L.A., Brown, T.T., Huggins, D.R., 2014. LiDAR based biomass and crop nitrogen estimates for rapid, non-destructive assessment of wheat nitrogen status. F. Crop. Res. 159, 21–32. https://doi.org/10.1016/J.FCR.2014.01.008.

Fischler, M.A., Bolles, R.C., 1981. Random sample consensus: a paradigm for model fitting with applications to image analysis and automated cartography. Commun. ACM 24, 381–395. https://doi.org/10.1145/358669.358692.

Fitzgibbon, A., Pilu, M., Fisher, R.B., 1999. Direct least square fitting of ellipses. IEEE Trans. Pattern Anal. Mach. Intell. 21, 476–480. https://doi.org/10.1109/34.765658.

Frasson, R.P. de M., Krajewski, W.F., 2010. Three-dimensional digital model of a maize plant. Agric. For. Meteorol. 150, 478–488. https://doi.org/10.1016/J.AGRFORMET.2010.01.003.

Furbank, R.T., Tester, M., 2011. Phenomics – technologies to relieve the phenotyping bottleneck. Trends Plant Sci. 16, 635–644. https://doi.org/10.1016/J.TPLANTS.2011.09.005.

Garrido, M., Paraforos, D., Reiser, D., Vázquez Arellano, M., Griepentrog, H., Valero, C., Garrido, M., Paraforos, D.S., Reiser, D., Vázquez Arellano, M., Griepentrog, H.W., Valero, C., 2015. 3D maize plant reconstruction based on georeferenced overlapping LiDAR point clouds. Remote Sens. 7, 17077–17096. https://doi.org/10.3390/rs71215870.

Gebbers, R., Ehlert, D., Adamek, R., 2011. Rapid mapping of the leaf area index in agricultural crops. Agron. J. 103, 1532. https://doi.org/10.2134/agronj2011.0201.

George-Jaeggli, B., Jordan, D.R., van Oosterom, E.J., Hammer, G.L., 2011. Decrease in sorghum grain yield due to the dw3 dwarfing gene is caused by reduction in shoot biomass. F. Crop. Res. 124, 231–239. https://doi.org/10.1016/J.FCR.2011.07.005.

Gibbs, J.A., Pound, M., French, A.P., Wells, D.M., Murchie, E., Pridmore, T., 2018. Plant phenotyping: an active vision cell for three-dimensional plant shoot reconstruction. Plant Physiol. 178, 524–534. https://doi.org/10.1104/pp.18.00664.

Holz, D., Ichim, A.E., Tombari, F., Rusu, R.B., Behnke, S., 2015. Registration with the point cloud library: a modular framework for aligning in 3-D. IEEE Robot. Autom. Mag. 22, 110–124. https://doi.org/10.1109/MRA.2015.2432331.

Hu, Y., Wang, L., Xiang, L., Wu, Q., Jiang, H., Hu, Y., Wang, L., Xiang, L., Wu, Q., Jiang, H., 2018. Automatic non-destructive growth measurement of leafy vegetables based on kinect. Sensors 18, 806. https://doi.org/10.3390/s18030806.

Jay, S., Rabatel, G., Hadoux, X., Moura, D., Gorretta, N., 2015. In-field crop row phenotyping from 3D modeling performed using Structure from Motion. Comput. Electron. Agric. 110, 70–77. https://doi.org/10.1016/J.COMPAG.2014.09.021.

Jiang, Y., Li, C., Paterson, A.H., 2016. High throughput phenotyping of cotton plant height using depth images under field conditions. Comput. Electron. Agric. 130, 57–68. https://doi.org/10.1016/J.COMPAG.2016.09.017.

Jiang, Y., Li, C., Paterson, A.H., Sun, S., Xu, R., Robertson, J., 2018. quantitative analysis of cotton canopy size in field conditions using a consumer-grade RGB-D camera. Front. Plant Sci. 8, 2233. https://doi.org/10.3389/fpls.2017.02233.

Kaminuma, E., Heida, N., Tsumoto, Y., Yamamoto, N., Goto, N., Okamoto, N., Konagaya, A., Matsui, M., Toyoda, T., 2004. Automatic quantification of morphological traits via three-dimensional measurement of Arabidopsis. Plant J. 38, 358–365. https://doi.org/10.1111/j.1365-313X.2004.02042.x.

Kruskal, J.B., 1956. On the shortest spanning subtree of a graph and the traveling salesman problem. Proc. Am. Math. Soc. 7, 48–48. https://doi.org/10.1090/S0002-9939-1956-0078686-7.

Li, J., Tang, L., 2018. Crop recognition under weedy conditions based on 3D imaging for robotic weed control. J. F. Robot. 35, 596–611. https://doi.org/10.1002/rob.21763.

Li, L., Zhang, Q., Huang, D., Li, L., Zhang, Q., Huang, D., 2014. A review of imaging techniques for plant phenotyping. Sensors 14, 20078–20111. https://doi.org/10.3390/s141120078.

Lu, H., Tang, L., Whitham, S.A., Mei, Y., 2017. A robotic platform for corn seedling morphological traits characterization. Sensors (Basel) 17. https://doi.org/10.3390/s17092082.

Marton, Z.C., Rusu, R.B., Beetz, M., 2009. On fast surface reconstruction methods for large and noisy point clouds. In: 2009 IEEE International Conference on Robotics and Automation. IEEE, pp. 3218–3223. https://doi.org/10.1109/ROBOT.2009.5152628.

McCormick, R.F., Truong, S.K., Mullet, J.E., 2016. 3D sorghum reconstructions from depth images identify QTL regulating shoot architecture. Plant Physiol. 172, 823–834. https://doi.org/10.1104/pp.16.00948.

Neilson, E.H., Edwards, A.M., Blomstedt, C.K., Berger, B., Møller, B.L., Gleadow, R.M., 2015. Utilization of a high-throughput shoot imaging system to examine the dynamic phenotypic responses of a C4 cereal crop plant to nitrogen and water deficiency over time. J. Exp. Bot. 66, 1817–1832. https://doi.org/10.1093/jxb/eru526.

Nguyen, T., Slaughter, D., Max, N., Maloof, J., Sinha, N., Nguyen, T.T., Slaughter, D.C., Max, N., Maloof, J.N., Sinha, N., 2015. Structured light-based 3D reconstruction system for plants. Sensors 15, 18587–18612. https://doi.org/10.3390/s150818587.

Paulus, S., Behmann, J., Mahlein, A.K., Plümer, L., Kuhlmann, H., 2014a. Low-cost 3D systems: suitable tools for plant phenotyping. Sensors (Switzerland) 14, 3001–3018. https://doi.org/10.3390/s140203001.

Paulus, S., Dupuis, J., Mahlein, A.-K., Kuhlmann, H., 2013. Surface feature based classification of plant organs from 3D laserscanned point clouds for plant phenotyping. BMC Bioinf. 14, 238. https://doi.org/10.1186/1471-2105-14-238.

Paulus, S., Dupuis, J., Riedel, S., Kuhlmann, H., Paulus, S., Dupuis, J., Riedel, S., Kuhlmann, H., 2014b. Automated analysis of barley organs using 3D laser scanning: an approach for high throughput phenotyping. Sensors 14, 12670–12686. https://doi.org/10.3390/s140712670.

Phillips, R.L., 2010. Mobilizing science to break yield barriers. Crop Sci. 50, S-99. https://doi.org/10.2135/cropsci2009.09.0525.

Pound, M.P., French, A.P., Murchie, E.H., Pridmore, T.P., 2014. Automated recovery of three-dimensional models of plant shoots from multiple color images. Plant Physiol.

166, 1688–1698. https://doi.org/10.1104/pp.114.248971.
Rosell Polo, J.R., Sanz, R., Llorens, J., Arnó, J., Escolà, A., Ribes-Dasi, M., Masip, J., Camp, F., Gràcia, F., Solanelles, F., Pallejà, T., Val, L., Planas, S., Gil, E., Palacín, J., 2009. A tractor-mounted scanning LIDAR for the non-destructive measurement of vegetative volume and surface area of tree-row plantations: a comparison with conventional destructive measurements. Biosyst. Eng. 102, 128–134. https://doi.org/10.1016/J.BIOSYSTEMSENG.2008.10.009.
Rovira-Más, F., Zhang, Q., Reid, J.F., 2005. Creation of three-dimensional crop maps based on aerial stereoimages. Biosyst. Eng. 90, 251–259. https://doi.org/10.1016/J.BIOSYSTEMSENG.2004.11.013.
Rusu, R.B., Cousins, S., 2011. 3D is here: Point Cloud Library (PCL). In: 2011 IEEE International Conference on Robotics and Automation. IEEE, pp. 1–4. https://doi.org/10.1109/ICRA.2011.5980567.
Salas Fernandez, M.G., Bao, Y., Tang, L., Schnable, P.S., 2017. A high-throughput, field-based phenotyping technology for tall biomass crops. Plant Physiol. 174, 2008–2022. https://doi.org/10.1104/pp.17.00707.
Sodhi, P., Vijayarangan, S., Wettergreen, D., 2017. In-field segmentation and identification of plant structures using 3D imaging. In: 2017 IEEE/RSJ International Conference on Intelligent Robots and Systems (IROS). IEEE, pp. 5180–5187. https://doi.org/10.1109/IROS.2017.8206407.
Sun, S., Li, C., Paterson, A., Sun, S., Li, C., Paterson, A.H., 2017. In-field high-throughput phenotyping of cotton plant height using LiDAR. Remote Sens. 9, 377. https://doi.org/10.3390/rs9040377.
Tang, H., Brolly, M., Zhao, F., Strahler, A.H., Schaaf, C.L., Ganguly, S., Zhang, G., Dubayah, R., 2014. Deriving and validating Leaf Area Index (LAI) at multiple spatial scales through lidar remote sensing: a case study in Sierra National Forest, CA. Remote Sens. Environ. 143, 131–141. https://doi.org/10.1016/J.RSE.2013.12.007.
Tilman, D., Balzer, C., Hill, J., Befort, B.L., 2011. Global food demand and the sustainable intensification of agriculture. Proc. Natl. Acad. Sci. USA 108, 20260–20264. https://doi.org/10.1073/pnas.1116437108.
White, J.W., Andrade-Sanchez, P., Gore, M.A., Bronson, K.F., Coffelt, T.A., Conley, M.M., Feldmann, K.A., French, A.N., Heun, J.T., Hunsaker, D.J., Jenks, M.A., Kimball, B.A., Roth, R.L., Strand, R.J., Thorp, K.R., Wall, G.W., Wang, G., 2012. Field-based phenomics for plant genetics research. F. Crop. Res. 133, 101–112. https://doi.org/10.1016/J.FCR.2012.04.003.
Xin, Z., Li Wang, M., Barkley, N.A., Burow, G., Franks, C., Pederson, G., Burke, J., 2008. Applying genotyping (TILLING) and phenotyping analyses to elucidate gene function in a chemically induced sorghum mutant population. BMC Plant Biol. 8, 103. https://doi.org/10.1186/1471-2229-8-103.
Yang, W., Guo, Z., Huang, C., Duan, L., Chen, G., Jiang, N., Fang, W., Feng, H., Xie, W., Lian, X., Wang, G., Luo, Q., Zhang, Q., Liu, Q., Xiong, L., 2014. Combining high-throughput phenotyping and genome-wide association studies to reveal natural genetic variation in rice. Nat. Commun. 5, 5087. https://doi.org/10.1038/ncomms6087.
Zhang, X., Huang, C., Wu, D., Qiao, F., Li, W., Duan, L., Wang, K., Xiao, Y., Chen, G., Liu, Q., Xiong, L., Yang, W., Yan, J., 2017. High-throughput phenotyping and qtl mapping reveals the genetic architecture of maize plant growth. Plant Physiol. 173, 1554–1564. https://doi.org/10.1104/pp.16.01516.